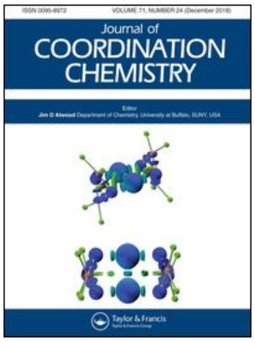

Taylor & Francis
Taylor & Francis Group

Journal of Coordination Chemistry

ISSN: 0095-8972 (Print) 1029-0389 (Online) Journal homepage: https://www.tandfonline.com/loi/gcoo20

Ferrocenyl induced one-pot synthesis of 3,3'-ferrocenylbiindoles

Ligang Yan, Limin Han & Ruijun Xie

To cite this article: Ligang Yan, Limin Han & Ruijun Xie (2020): Ferrocenyl induced one-pot synthesis of 3,3′-ferrocenylbiindoles, Journal of Coordination Chemistry, DOI: 10.1080/00958972.2020.1770235

To link to this article: https://doi.org/10.1080/00958972.2020.1770235

JOURNAL OF COORDINATION CHEMISTRY
https://doi.org/10.1080/00958972.2020.1770235

Ferrocenyl induced one-pot synthesis of 3,3′-ferrocenylbiindoles

Ligang Yan, Limin Han and Ruijun Xie

Chemical Engineering College, Inner Mongolia University of Technology, Hohhot, P. R. China

ABSTRACT

When we used 2-ferrocenethynylaniline (**1a**) as reactant and $NaAuCl_4 \cdot 2H_2O$ (5%) as catalyst to prepare 2-ferrocenylindole (**2a**), we were surprised to find that 3,3′-ferrocenylbiindole (**3a**) was obtained simultaneously. **3a** was characterized by elemental analysis, FT-IR, MS, NMR, and X-ray single crystal diffraction. The reactant substitution reaction, *in-situ* HNMR, XPS, EPR characterization, and calculations were carried out to interpret why **3a** was obtained in one pot. The results showed that the hydroperoxyl radical played a key role in the reaction, which induced synthesis of **3a**.

ARTICLE HISTORY
Received 22 January 2020
Accepted 29 April 2020

KEYWORDS
Ferrocenyl; biindoles; one-pot synthesis; reaction mechanism; homo-coupling

---

CONTACT Limin Han hanlimin_442@hotmail.com Chemical Engineering College, Inner Mongolia University of Technology, Hohhot 010051, P. R. China

Supplemental data for this article can be accessed https://doi.org/10.1080/00958972.2020.1770235.

1. Introduction

The indole nucleus is a common substructure of many natural products and pharmaceutical compounds, found in calycanthidine, chimonanthine, psychotriasine, melatonin, and tryptophan [1–4]. Synthesis methods of indole and its derivatives, such as Fischer indole synthesis, cyclization of 2-alkynylaniline, and reductive cyclizations of nitro compounds [5], have been studied extensively. Transition metal-catalyzed C–H activation of indoles also played important roles for the synthesis of indole derivatives, for example, palladium-catalyzed electrophilic substitution reaction of indole and umpolung of 2-indolylmethanols can be used to construct a large number of indole derivatives [6–12].

Recently, the synthesis of biindole derivatives, such as 6,6′-biindole,3,3′-biindole, biindole-methane [13–15], has attracted much attention. Up to now, the construction of biindolyl compounds can be classified into three main methods. First, the biindoles can be formed through oxidative dimerization of indoles (Scheme 1(a)) [16–19]; secondly, the biindoles can be constructed by transitional metal-catalyzed coupling reaction or substitution reaction of pre-functionalized indole [20–25] (Scheme 1(b) and (c)); shirdly, the cyclization reaction and C–H oxidative homo-coupling reaction of the 2-alkynylanilines (Scheme 1(d)) [26, 27]. Overall, one-pot synthesis of diindole from 2-alkynylanilines is an economical method, but the synthesis mechanism of diindole still needs to be further studied.

Ferrocene has a stereoscopic sandwich structure and redox properties. Therefore, if a heterocyclic compound involves ferrocene units, it may exhibit some unique chemical properties [28, 29]. Despite our research group having synthesized many ferrocenyl heterocyclic compounds [30], we want to synthesize the rare ferrocenyl indole compounds.

First, we want to use Au-catalyzed cyclization of 2-ferrocenethynylaniline (**1a**) to synthesize ferrocenyl indoles (**2a**) [31, 32]. Interestingly, the target product was not the desired product **2a**, but 3,3′-ferrocenylbiindole (**3a**) was obtained. Hence, we interpret why **3a** was obtained in one pot. Through reactant–substitution reaction, *in-situ* HNMR characterization, XPS, EPR characterization, and theory calculations, we propose a ferrocenyl-induced hydroperoxyl radical catalytic mechanism in this article.

2. Experimental

2.1. General procedures

All the reactions were monitored with thin-layer chromatography (TLC). $NaAuCl_4{\cdot}2H_2O$, 2-iodoaniline, 2-phenylethynylaniline (**1b**), 2-phenylindole (**2b**), ferrocenylacetylene, NH_4Cl, and K_2CO_3 were commercially available. Column chromatographic separations and purifications were performed on 100–200 mesh silica gel. ^1H and ^{13}C spectra were recorded on an Agilent Technologies-500 MHz spectrometer. FT-IR spectra were measured on a Nexus-870 FT-IR spectrometer. Elemental analyses were carried out on an Elementarvar III-type analyzer. Mass spectra were determined using a Shimadzu LCMS-2020 instrument. X-ray photoelectron spectra (XPS) and valence bond spectra (VBS)

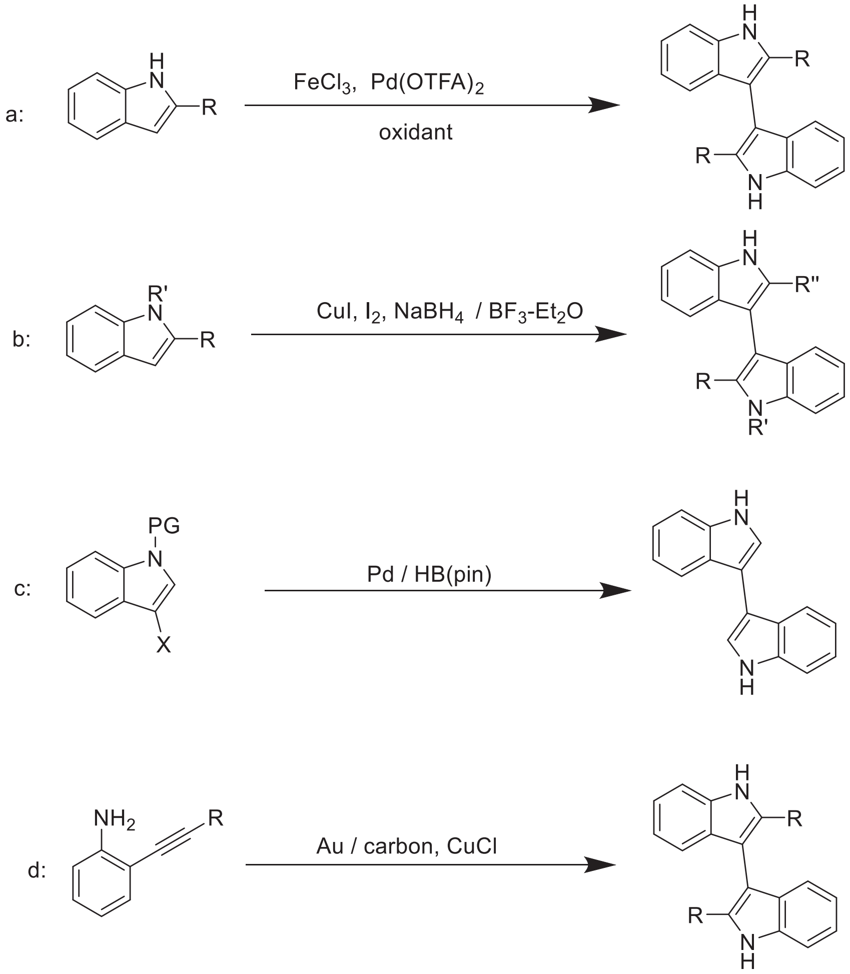

Scheme 1. The synthesis of 3,3′-biindoles.

were measured on a Thermo-Fisher ESCALAB 250Xi spectrometer equipped with a monochromatic Al X-ray source (1486.6 eV). Electron paramagnetic resonance (EPR) was measured using a Bruker EPR spectrometer (A300, X band) with the microwave frequency 9.5 GHz and modulation frequency (100 kHz). Theory calculations were performed using Gaussian09 [33]. The geometry optimizations, frequency analysis, and thermodynamic corrections were performed at the B3LYP (D3BJ), MDF10 (for Fe), and Def2SVP (for others) level of theory [34–36].

2.2. Synthesis

2.2.1. Synthesis of 2-ferrocenethynylaniline (1a)

An ethanol solution (10 mL) containing 2-iodoaniline (88 mg, 0.4 mmol), ferrocenylacetylene (42 mg, 0.2 mmol), PdCl{[(η^5-C_5H_5)]Fe[(η^5-C_5H_3)]-2-Py}(Py)] (3 mg, 0.005 mmol), and K_2CO_3 (57 mg, 0.4 mmol) was stirred at 40 °C for 4 h under an argon atmosphere (Scheme 2). The reaction mixture was washed with degassed water and extracted with

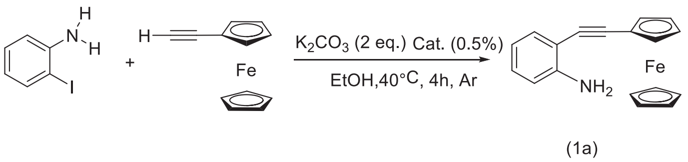

Scheme 2. The synthesis of 2-ferrocenethynylaniline.

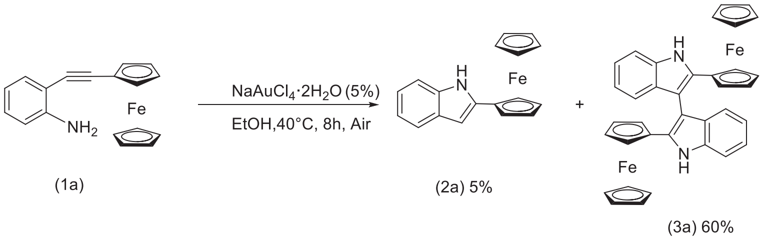

Scheme 3. The synthesis of 3,3′-ferrocenylbiindole.

dichloromethane. The organic layer was filtered and the solvent was removed under vacuum. The residue was subjected to chromatographic separation on a silica gel column (2.0 × 30 cm). Elution with a mixture of dichloromethane and hexane (1:2/V:V) gave the second red band as **1a**. Single crystals of **1a** were obtained from a mixture of hexane:dichloromethane (3:1/V:V).

2-Ferrocenethynylaniline (**1a**) Yield: 39 mg, 65%. M.p. 123–125 °C (decomp). Anal. Calcd for $C_{18}H_{15}FeN$: C, 71.76%; H, 4.98%; N, 4.65%. Found: C, 72.06%; H, 5.53%; N, 4.98%. FT-IR (cm^{-1}): 3472, 3374, 3090, 2921, 2201, 1605, 1446, 1308, 1161, 815, 752. ^1H NMR (500 MHz, $CDCl_3$): δ: 7.35 (d, 1H, $J = 7.5$ Hz, Ph), 7.13 (t, 1H, $J = 8$ Hz, Ph), 6.72 (m, 2H, Ph), 4.52 (s, 2H, Cp), 4.25 (s, 7H, Cp), 3.99 (s, 1H, NH_2) ppm. ^{13}C NMR (125 MHz, $CDCl_3$): δ: 131.85, 129.12, 118.05, 114.33, 93.55, 81.99, 71.34, 69.95, 68.87, 65.91. ESI-MS (CH_2Cl_2, *m/z*): 300.95 (M^+).

2.2.2. Synthesis of 2-ferrocenylindole (2a) and 3,3′-ferrocenylbiindole (3a)

2-Ferrocenethynylaniline (**1a**) (60 mg, 0.2 mmol) and $NaAuCl_4·2H_2O$ (5%) (4 mg, 0.01 mmol) were dissolved in ethanol (5 mL) and stirred at 40 °C for 8 h in air (Scheme 3). Then, the reaction mixture was quenched with saturated NH_4Cl solution and extracted with dichloromethane. The organic solvent was removed *in vacuo* and the residues were subjected to chromatographic separation on a silica gel column (2.0 × 30 cm). Elution with a mixture of dichloromethane and hexane (1:2/V:V) gave the first yellow band as **2a**. The second orange band was **3a**; single crystals of **3a** were obtained from a mixture of hexane:dichloromethane (3:1/V:V).

2-Ferrocenylindole (**2a**), Yield: 3 mg, 5%. M.p. 168–170 °C (decomp). Anal. Calcd for $C_{18}H_{15}FeN$: C, 71.76%; H, 4.98%; N, 4.65%. Found: C, 72.01%; H, 5.15%; N, 5.01%. FT-IR (cm^{-1}, KBr): 3435, 1443, 1417, 1344, 1293, 1105, 1029, 819, 791, 734. ^1H NMR (500 MHz, $CDCl_3$): δ: 8.05 (bs, 1H, N–H), 7.55 (d, 1H, $J = 7.5$ Hz, Ph), 7.36 (d, 1H,

$J = 8.0$ Hz, Ph), 7.15 (t, 1H, $J = 7$ Hz, Ph), 7.09 (t, 1H, $J = 7.5$ Hz, Ph), 6.52 (s, 1H, pyrrole), 4.64 (s, 2H, C_5H_4), 4.34 (s, 2H, C_5H_4), 4.11 (s, 5H, C_5H_5) ppm. ^{13}C NMR (125 MHz, $CDCl_3$): δ: 137.06, 136.23, 129.34, 121.39, 119.97, 119.78, 110.33, 98.88, 69.55, 68.82, 65.91. ESI-MS (CH_2Cl_2, *m/z*): 300.95 (M^+).

3,3′-Ferrocenylbiindole (**3a**), Yield: 36 mg, 60%. M.p. 115–118 °C (decomp). Anal. Calcd for $C_{36}H_{28}Fe_2N_2$: C, 71.76%; H, 4.65%; N, 4.65%. Found: C, 72.21%; H, 4.88%; N, 5.05%. FT-IR (cm^{-1}): 3473, 3091, 1608, 1592, 1494, 1461, 1447, 1309, 1164, 818, 754. ^{1}H NMR (500 MHz, $CDCl_3$): δ: 7.36 (d, 2H, $J = 8$ Hz, Ph), 7.13 (t, 2H, $J = 7.5$ Hz, Ph), 6.86 (d, 2H, $J = 7.5$ Hz, Ph), 6.77 (d, 2H, $J = 7.5$ Hz, Ph), 4.52 (s, 4H, C_5H_4), 4.23 (s, 14H, C_5H_4, C_5H_5) ppm. ^{13}C NMR (125 MHz, $CDCl_3$): δ: 147.30, 131.75, 129.07, 117.76, 114.56, 93.56, 81.76, 71.27, 69.92, 68.88, 65.09. ESI-MS (CH_2Cl_2, *m/z*): 599.95 (M^+).

2.2.3. Synthesis of 2-phenylindole (2b) and diphenylbiindole (3b)

2-Phenylethynylaniline (**1 b**) (39 mg, 0.2 mmol), ferrocene (19 mg, 0.1 mmol), and $NaAuCl_4 \cdot 2H_2O$ (5%) (4 mg, 0.01 mmol) were dissolved in ethanol (5 mL) and stirred at 40 °C for 8 h under air or 70 °C for 24 h under oxygen. After the reaction was completed, the reaction mixture was extracted by dichloromethane. The organic solvent was removed *in vacuo* and the residues were subjected to chromatographic separation on a silica gel column (2.0×30 cm). Elution with a mixture of dichloromethane and hexane (1:3/V:V) gave the corresponding pure product **2b** (in air) and **3b** (in oxygen). The spectroscopic data were consistent with those reported previously [26].

2-Phenylindole (**2b**): ^{1}H NMR (500 MHz, $CDCl_3$): δ: 8.31 (s, 1H, NH), 7.67–7.62 (m, 3H, ArH), 7.45–7.39 (m, 3H, ArH), 7.32 (t, 1H, $J = 6.5$ Hz, ArH), 7.20 (t, 1H, $J = 2.5$ Hz, ArH), 7.12 (t, 1H, $J = 9$ Hz, ArH), 6.83 (s, 1H, C-3H) ppm. ^{13}C NMR (125 MHz, $CDCl_3$): δ: 137.9, 132.4, 129.2, 127.7, 125.2, 122.4, 120.7, 120.3, 110.1, 100.0.

Diphenylbiindole (**3b**): ^{1}H NMR (500 MHz, DLM): δ: 10.65 (s, 2H, NH), 7.55 (d, 4H, $J = 7.5$ Hz, ArH), 7.49 (d, 2H, $J = 8$ Hz, ArH), 7.15–7.03 (m, 10H, ArH), 6.87 (t, 2H, $J = 7.5$ Hz, ArH) ppm. ^{13}C NMR (125 MHz, DLM): δ: 137.6, 135.5, 133.9, 130.7, 129.2, 127.7, 127.4, 122.5, 120.3, 119.6, 111.9, 107.5.

2.3. X-ray crystallography

X-ray single crystal data for **1a** and **3a** were recorded on a Bruker APEX II CCD diffractometer with graphite-monochromated Mo Ka ($k = 0.71073$ Å) radiation [37]. Empirical absorption corrections by semi-empirical methods from equivalents were carried out. The structures were solved by direct methods using SHELXS-97 and refined with SHELXL-97 by full-matrix least-squares techniques on F^2 [38]. All non-hydrogen atoms were refined anisotropically, while the hydrogens were located geometrically and refined isotropically.

3. Results and discussion

3.1. Synthesis and characterizations of 1a, 2a, and 3a

Compounds **1a** and **3a** were synthesized and their molecular structures were characterized by NMR, FT-IR, and X-ray single crystal diffraction. According to the gold-

Table 1. Crystal data and relevant structural parameters of **1a** and **3a**.

	1a	3a
Formula	$C_{18}H_{15}FeN$	$C_{37}H_{30}Cl_2Fe_2N_2$
Formula weight	301.16	685.23
T/°C	20(2)	20(2)
λ/Å	0.71073	0.71073
Crystal system	Monoclinic	Monoclinic
Space group	$P2_1/c$	$P2_1/c$
a/Å	9.2634(4)	12.8235(9)
b/Å	10.6602(5)	15.5818(11)
c/Å	14.6444(7)	9.1541(7)
α/°	90	90
β/°	106.272(2)	99.475(2)
γ/°	90	90
V/Å^3	1388.20(11)	3044.2(2)
Z	4	4
ρ_{Calcd}/g m^{-3}	1.441	1.495
Abs. coeff./mm^{-1}	1.074	1.159
F(0 0 0)	624	1408.0
2θ range/°	5.796–56.808	5.77–52.836
Reflections collected	27,514	49,806
Unique	3471	6231
Completeness to θ	99.5%	99.9%
$T_{\text{max.}}$ and $T_{\text{min.}}$	0.746 and 0.600	0.578 and 0.573
Goodness-of-fit on F^2	1.065	1.041
Final R indices [$I > 2\sigma(I)$]	$R1 = 0.0549$	$R1 = 0.1221$,
R indices (all data)	$wR2 = 0.1263$,	$wR2 = 0.2692$,
	$R1 = 0.0732$,	$R1 = 0.1547$,
	$wR2 = 0.1369$	$wR2 = 0.2922$

catalyzed protocol in the literature [39], for the $NaAuCl_4 \cdot 2H_2O$-catalyzed cyclization of **1a**, the desired **2a** should be obtained. But in the present preparation, we were surprised to find that **3a** was obtained in good yield (Scheme 3). The ^1H and ^{13}C NMR spectra of **1a** and **3a** were similar in $CDCl_3$. The chemical shift of the two protons of the substituted Cp-rings appeared at $\delta = 4.50$–4.53 ppm, whereas the other seven protons of Cp rings appeared at $\delta = 4.23$–4.25 ppm. Protons of the benzene groups appeared at $\delta = 7.35$, 7.13, and 6.72 ppm, respectively. But the protons of amino groups (**1a**) were at $\delta = 3.99$ ppm, which could be used to distinguish **1a** and **3a** in NMR spectra [26]. The molecular structures of **1a** and **3a** were further confirmed by X-ray single crystal diffraction analysis. Crystal data and relevant structural parameters are listed in Table 1. Selected bond lengths and angles are listed in Table 2. ORTEP diagrams of **1a** and **3a** are shown in Figures 1 and 2. Owing to the formation of a pyrrole ring *via* cyclization, the bond lengths of the C–N and C–C in **1a** are shorter than the corresponding bond lengths in **3a**. For instance, the N(1)–C(18) bond length is 1.331(5) Å and the C(11)–C(12) bond length is 1.197(4) Å in **1a**. The N(2)–C(25) bond length is 1.372(11) Å, the N(1)–C(12) bond length is 1.366(13) Å and the C(11)–C(18) bond length is 1.355(12) Å in **3a**. In the crystal structure of **3a**, because the bond length of the two pyrrole rings were different, the dihedral angles between the one pyrrole ring (C18–C17–C12–N1) and the Fc ring is 19.688° while the dihedral angles between another pyrrole ring (C20–C19–C26–N2) and the Fc ring is 4.224°. The dihedral angle of the two pyrrole rings was 81.586°, which was the axially chiral 3,3′-bisindole frameworks due to introducing the Fc group. The molecular structure of **2a** can be further determined by the 2D COSY, 2D HSQC, and 2D HMQC (see Supporting Information). $\delta = 8.05$ ppm and $\delta = 6.52$ showed no spatial correlation with other protons. The $\delta = 8.05$ ppm is attributed to the

Table 2. Selected bond lengths (Å) and angles (°) of **1a** and **3a**.

1a		3a	
Fe(1)–C(10)	2.045(3)	N(1)–C(11)	1.392(10)
Fe(1)–C(6)	2.034(3)	N(1)–C(12)	1.366(13)
C(11)–C(10)	1.432(4)	C(11)–C(18)	1.355(12)
C(11)–C(12)	1.197(4)	N(2)–C(26)	1.379(10)
N(1)–C(18)	1.331(5)	C(19)–C(18)	1.469(11)
C(12)–C(14)	1.455(5)	N(2)–C(25)	1.372(11)
C(11)–C(10)–C(6)	125.4(3)	C(18)–C(19)–C(26)	128.3(7)
C(18)–C(14)–C(12)	118.9(3)	C(17)–C(18)–C(19)	125.9(8)
N(1)–C(18)–C(14)	120.7(4)	C(10)–C(11)–C(18)	130.5(7)
C(11)–C(12)–C(14)	179.6(4)	C(18)–C(19)–C(20)	125.8(7)
C(9)–C(8)–C(7)	108.3(3)	C(27)–C(26)–C(19)	130.5(7)
C(14)–C(13)–C(15)	118.7(4)	C(19)–C(20)–C(25)	108.2(7)

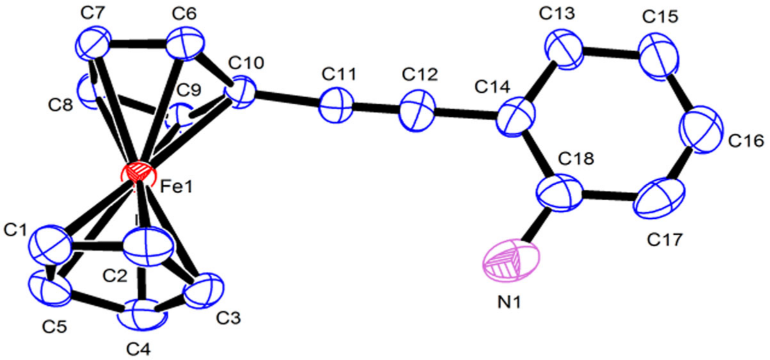

Figure 1. The molecular structure of **1a**. Hydrogens have been omitted for clarity.

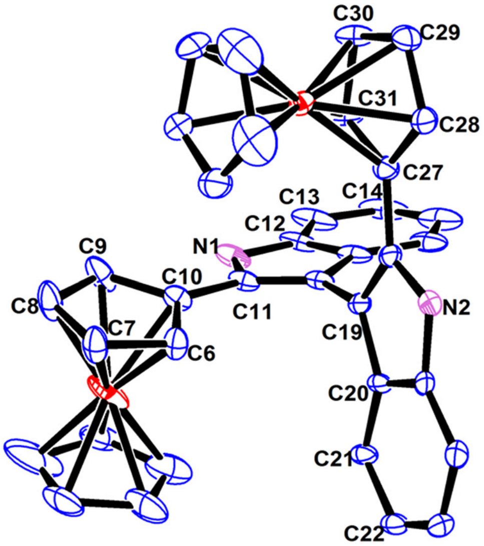

Figure 2. The molecular structure of **3a**. Hydrogens have been omitted for clarity.

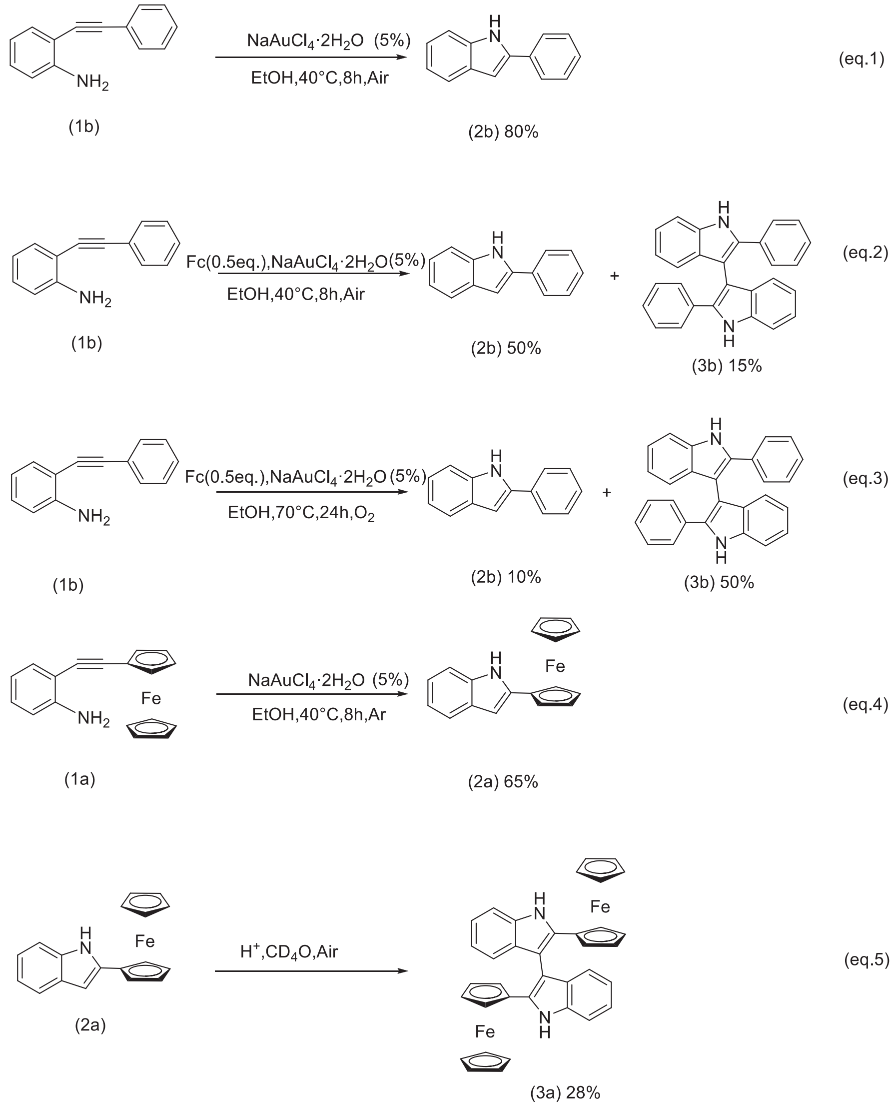

Scheme 4. Primary mechanism studies.

H-1 protons. The $\delta = 6.52$ ppm corresponded to the H-3 of pyrrole. In order to distinguish the H-1 and H-3 protons accurately, the chemical shift of 8.05 ppm disappeared in 2D HSQC, illustrating that the chemical shifts of H-3 of pyrrole was 6.52 ppm. Through analysis of 2D COSY, 2D HSQC, and 2D HMQC, the chemical shifts of H-5, H-8, H-7, and H-6 protons were at $\delta = 7.53$, 7.35, 7.14, and 7.09 ppm, respectively. The protons of the ferrocenyl units were at $\delta = 4.11$ ppm (C_5H_5), 4.34 ppm, and 4.64 ppm (C_5H_4), respectively [32]. It is concluded that **2a** was synthesized.

3.2. Mechanism studies

In order to answer why 3,3′-ferrocenylbiindole (**3a**) can be obtained in one pot, several experiments were carried out (Scheme 4). First, we investigated the catalytic

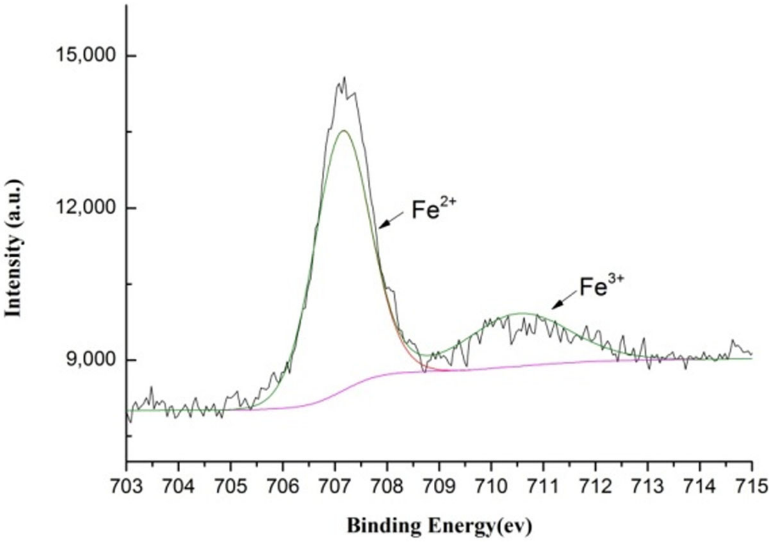

Figure 3. XPS Fe2$p_{3/2}$ spectra for the residues of reaction.

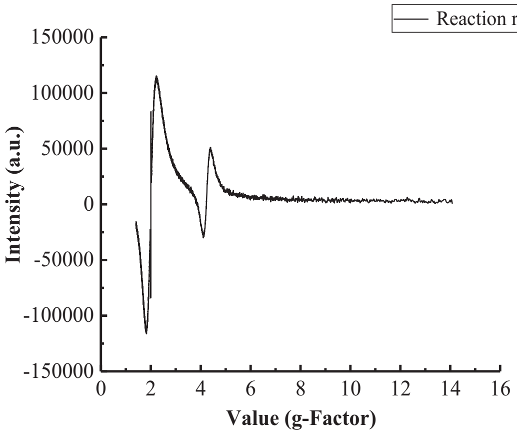

Figure 4. The EPR spectra for iron(III).

performance of Au for synthesizing the biindole. When 2-ferrocenethynylaniline (**1a**) was substituted by 2-phenylethynylaniline (**1b**) under the standard reaction conditions, only 2-phenylindole (**2b**) was obtained in 80% yield (Scheme 4, eq. 1). This demonstrates that $NaAuCl_4 \cdot 2H_2O$ only catalyzes intramolecular cyclization reaction of **1b** to **2b**; $NaAuCl_4 \cdot 2H_2O$ could not catalyze oxidative coupling of **2b** to form 3,3′-diphenylbiindole (**3b**). With **1a** as reactant under the same reaction conditions, why was **3a** obtained? With this question, we investigated the synthesis of 3,3′-biindole derivatives extensively from the literature [16–27]. Fe^{3+} can catalyze oxidative homo-coupling of 2-arylindole to form the homo-coupling product 3,3′-biindole with molecular oxygen as the oxidant [18].

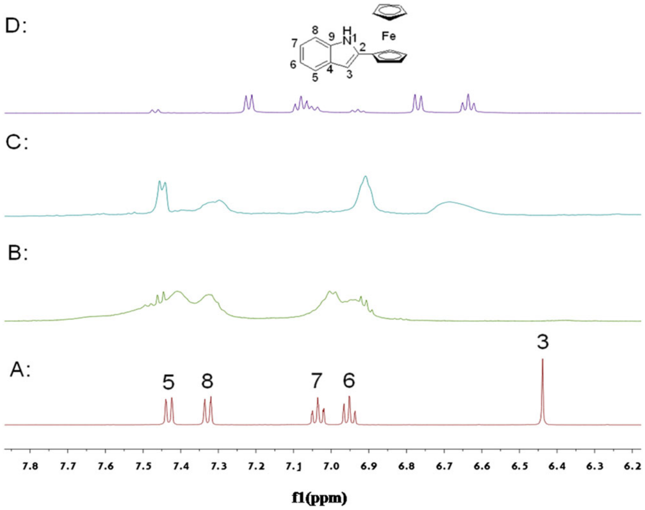

Figure 5. The proceeding of the reaction was determined by *in situ* ^{1}H NMR analysis of **2a** under air and acidity. ^{1}H NMR(CD_4O). (A) The ^{1}H NMR of **2a** when reaction starts in air. (B) The ^{1}H NMR of **2a** in acidic solution after 1 h. (C) The ^{1}H NMR of **2a** in acidic solution after 1 day. (D) The ^{1}H NMR of **3a**.

Ferrocene and ferrocenyl derivatives are classical acid-sensitive organometallics; under acidic media of $NaAuCl_4·2H_2O$–ethanol, the ferrocene will be oxidized to Fe^{3+} in oxygen or in air [40]. To test this, we repeated the reaction (Scheme 4, eq. 2) with the addition of ferrocene (0.5 eq.) under air and 3,3′-diphenylbiindole (**3b**) was obtained with yield of 15%. When the same reaction was performed under oxygen, the yield of **3b** increased to 50%. This phenomenon demonstrated that ferrocene could be the source of Fe^{3+} which was generated easily under oxygen atmosphere. Therefore, the Fe^{3+} and oxygen had key roles in oxidative homo-coupling reaction [18].

Is Fe^{3+} involved in the oxidative homo-coupling of **2a** to form **3a**? In order to obtain the valence of iron in the system, we used XPS to measure the surface chemical state of Fe species of the reaction residues (Scheme 3). There are two Fe $2p_{3/2}$ peaks, which could be described as mixed valence of Fe^{2+} and Fe^{3+} (Figure 3). The XPS binding energy for the 2p orbital of Fe^{2+} is about 707.5 eV relative to C 1s at 284.8 eV, while the binding energy for Fe^{3+} is about 710.7 eV. The Fe^{2+} signal may originate from the ferrocene moiety, while the Fe^{3+} can be attributed to the oxidation product of ferrocene [41]. The Fe^{3+} has also been confirmed by EPR spectroscopy of the reaction residues (Figure 4), where $g = 4.3$ (1500 G) is a characteristic value of Fe^{3+} [42].

Does Fe^{3+} come from the ferrocenyl of **1a** or **2a**? When **1a** is the reactant (Scheme 4, eq. 4), only **2a** was obtained under Ar atmosphere. This revealed that **2a** was synthesized through Au-catalyzed intramolecular cyclization of **1a**, and Fe^{3+} was not generated in argon. Under air atmosphere, **2a** (5%) and **3a** (60%) were obtained together (Scheme 3). These comparative experiments proved that air is necessary for formation of Fe^{3+}, which comes from ferrocene of **1a** or **2a**.

To investigate the effect of acid and air on the transformation of **2a** to **3a**, the *in situ* ^{1}H NMR experiment of **2a** was carried out under simulated reaction conditions

$$Fc \xrightarrow{+H^+ + O_2} Fe^{3+} + H\dot{O}_2 \quad (1)$$

$$H\dot{O}_2 + e^- + H^+ \longrightarrow H_2O_2 \quad (2)$$

$$Fe^{3+} + H_2O_2 \longrightarrow Fe^{2+} + H^+ + H\dot{O}_2 \quad (3)$$

$$Fc + H_2O_2 \longrightarrow Fc^+ + OH^- + H\dot{O} \quad (4)$$

Scheme 5. The redox reaction of ferrocene and its derivatives in air and acid condition.

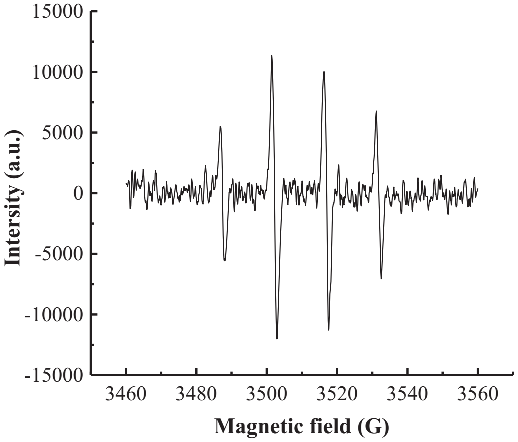

Figure 6. EPR spectra for DMPO adduct with **2a** (0.2 g/L) and HCl (25 mM) under atmospheric conditions.

with air and acidity (Scheme 4, eq. 5). The 6.43 ppm could be attributed to the chemical shift of **2a**. Initially, the 6.43 ppm was found in NMR spectra, which could be attributed to the chemical shift of the H-3 of pyrrole in **2a** (Figure 5(A)). With the addition of acid, the peaks disappeared at 6.43 ppm after 1 h (Figure 5(B)). As the reaction proceeded, the peaks at 7.5–7.2 ppm and 7.0–6.8 ppm gradually split and moved after 24 h (Figure 5(C)), in accord with the chemical shift of **3a** (Figure 5(D)). This result indicates that C–H bond cleavage at the C-3 position in **2a** could be key in the homo-coupling reaction to synthesize the desired **3a** through a single-electron-transfer pathway [18]. When Fe^{3+} was formed from the ferrocene of **1a** or **2a** under acid and air conditions, homo-coupling reaction was initiated.

Calculations were used to determine if Fe^{3+} was a real catalyst in the homo-coupling reaction. The redox reaction of ferrocene and its derivatives with air (or oxygen gas) in acidic solution have been done by several workers (Scheme 5) [43–46]. In C–H oxidative homo-coupling reaction, oxidants may be the radicals produced by oxidation of ferrocene and its derivatives. To verify this hypothesis, DMPO adduct with **2a** (0.2 g/L) and HCl (25 mM) were recorded under atmospheric conditions by EPR spectra. The result showed a strong four-line EPR signal with the relative intensity ratio of 1:2:2:1 (Figure 6) [45]. This illustrated that the addition of DMPO led to the EPR peak of DMPO-OH and the formation of hydroxyl radical (HO·) in the system. If the HO· was used as oxidant (Scheme 5, eqs. 1, 2, and 4), it would consume at least two equivalents of **2a** to produce one equivalent of **3a**. The yield of **3a** would be much lower than 50%. If the hydroperoxyl radical (HOO·) was utilized as oxidant (Scheme 5, eqs. 1, 2, and 3), one equivalent of

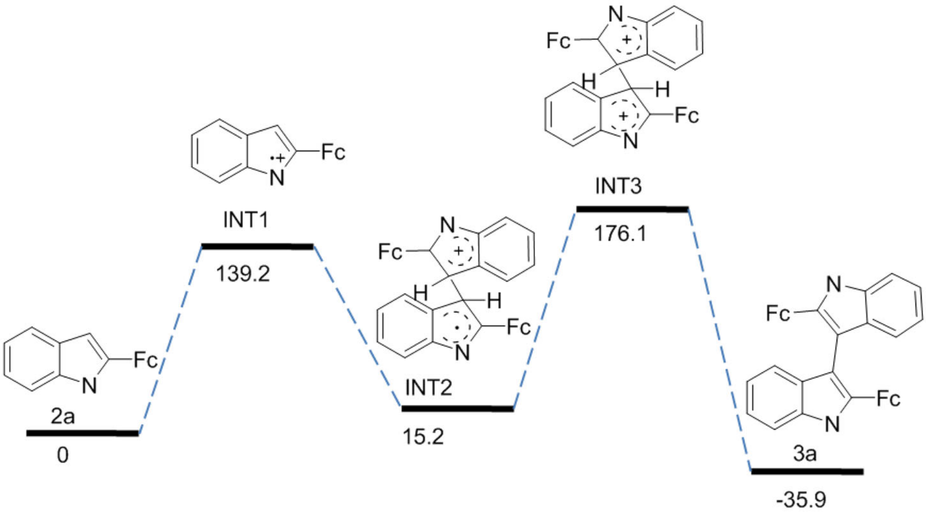

Figure 7. Energy profile for the reaction between **2a** and **3a**. Relative energies are given in kcal/mol.

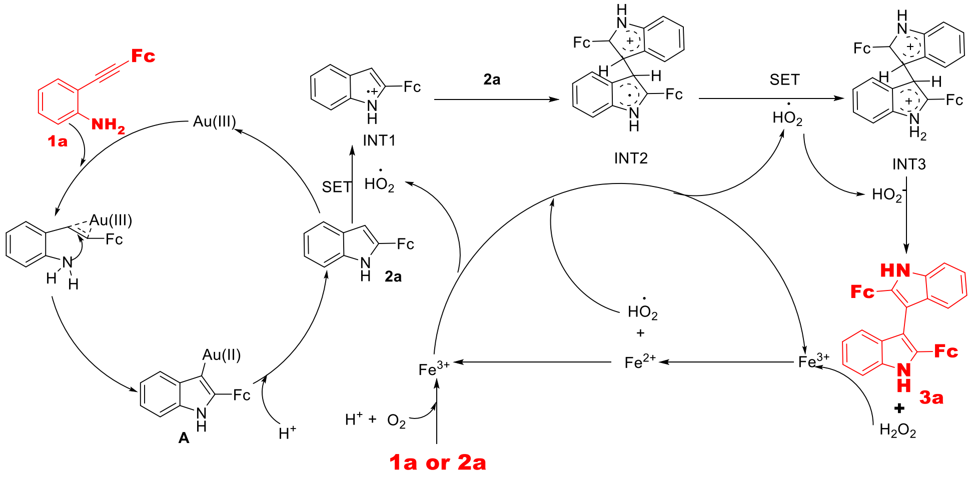

Scheme 6. Prospective catalytic cycle for the formation of 3,3′-ferrocenylbiindole.

2a would generate one equivalent of **3a**. Then, the yield of **3a** would be higher than 50%, but lower than 75%; the yield of **3a** was always 60–70% in this experiment. Comparing eq. 3 and eq. 4 in Scheme 5, the pH of the reaction system dominated the kinds of radicals. Strong acid promoted HO· in eq. 4; weak acid produced HOO· in eq. 3 [47]. In the EPR experiment, excessive acid led to the production of HO·.

To assess whether HOO· was involved in the C–H oxidative homo-coupling reaction, we complemented the mechanistic experimental with theoretical calculations (Figure 7). The relative free energy profile showed that there are three different intermediates in the process (INT1, INT2, and INT3). The highest energy intermediate (INT3) was 176.1 kcal/mol and the energy intermediate (INT1) was 139.2 kcal/mol above the reactants. The reason of the unusual high barrier was that the precursor of the intermediate

(INT3 or INT1) provided one electron to HOO· which would react with protons simultaneously (Scheme 5, eq. 2). For chemical calculation, this reaction was artificially divided into two stages, resulting in presenting the energy of half-reaction intermediates INT3 and INT1. When protons were involved in the reaction, the energy declined to −35.9 kcal/mol at the last step. The present experiments and calculations confirmed that HOO· was an oxidant in C–H oxidative homo-coupling reaction.

Based on the experiments, theory calculations, and the literature, a possible mechanism was proposed. The formation of **3a** may proceed *via* two steps (Scheme 6). The first step is the cyclization reaction initiated by the formation of the adduct between Au(III) and **1a** forming intermediate **A**. Then, intermediate **A** undergoes protonolysis to afford **2a** in the presence of strong acid [48]. The second step begins with generating of HOO· (Scheme 5, eq. 1); in eq. 1, the ferrocenyl of **1a** or **2a** was partially oxidized into Fe^{3+} by air and acid, HOO· was generated simultaneously. Then, HOO· captured an electron from another part of **2a** to form the radical cation intermediate INT1 which is then coupled to neutral **2a** to form intermediate INT2. Intermediate INT2 loses an electron to convert into intermediate INT3. Ultimately, deprotonation of INT3 leads to the corresponding **3a** [19].

4. Conclusion

We have synthesized a diindole compound, 3,3′-ferrocenylbiindoles (**3a**), and characterized it by elemental analysis, FT-IR, MS, NMR, and X-ray single crystal diffraction. We proposed a possible reaction mechanism through experiments and calculations. The research provides a new synthesis of biindole derivatives.

Disclosure statement

No potential conflict of interest was reported by the authors.

Funding

We are grateful to the Program for New Century Excellent Talents in University [NCET-08-858] and the Natural Science Foundation of China [NSFC-21462029].

References

[1] E.C. Gentry, L.J. Rono, M.E. Hale, R. Matsuura, R.R. Knowles. *J. Am. Chem. Soc.*, **140**, 3394 (2018).

[2] C.R. Jamison, J.J. Badillo, J.M. Lipshultz, R.J. Comito, D.W.C. MacMillan. *Nat. Chem.*, **9**, 1165 (2017).

[3] A.G. Turjanski, F. Leonik, D.A. Estrin, R.E. Rosenstein, F. Doctorovich. *J. Am. Chem. Soc.*, **122**, 10468 (2000).

[4] A. Crespo, A.G. Turjanski, D.A. Estrin. *Chem. Phys. Lett.*, **365**, 15 (2002).

[5] G.R. Humphrey, J.T. Kuethe. *Chem. Rev.*, **106**, 2875 (2006).

[6] S. Cacchi, G. Fabrizi. *Chem. Rev.*, **111**, PR215 (2011).

[7] S.W. Youn, T.Y. Ko. *Asian J. Org. Chem.*, **7**, 1467 (2018).

[8] V. Pirovano. *Eur. J. Org. Chem.*, **2018**, 1925 (2018).

[9] M.M. Xu, H.Q. Wang, Y.J. Mao, G.J. Mei, S.L. Wang, F. Shi. *J. Org. Chem.*, **83**, 5027 (2018).

[10] Z.Q. Zhu, Y. Shen, J.X. Liu, J.Y. Tao, F. Shi. *Org. Lett.*, **19**, 1542 (2017).

[11] B. Lu, Y.D. Luo, L.Z. Liu, L.W. Ye, Y.Z. Wang, L.M. Zhang. *Angew. Chem. Int. Ed. Engl.*, **50**, 8358 (2011).

[12] M. Sun, C. Ma, S.J. Zhou, S.F. Lou, J. Xiao, Y.C. Jiao, F. Shi. *Angew. Chem. Int. Ed. Engl.*, **58**, 8703 (2019).

[13] A.B. Gamble, P.A. Keller. *Chem. Commun. (Camb.)*, **46**, 4076 (2010).

[14] D.S. Black, N. Kumar. *Adv. Heterocycl. Chem.*, **101**, 97 (2010).

[15] Y. Wan, H.Q. Wang, M.M. Xu, G.J. Mei, F. Shi. *Org. Biomol. Chem.*, **16**, 1536 (2018).

[16] P.P. Huang, X.J. Peng, D. Hu, H.W. Liao, S.B. Tang, L.X. Liu. *Org. Biomol. Chem.*, **15**, 9622 (2017).

[17] Y. Li, W.H. Wang, S.D. Yang, B.J. Li, C. Feng, Z.J. Shi. *Chem. Commun. (Camb.)*, **46**, 4553 (2010).

[18] T.M. Niu, Y.H. Zhang. *Tetrahedron Lett.*, **51**, 6847 (2010).

[19] T. Wirtanen, M.K. Mäkelä, J. Sarfraz, P. Ihalainen, S. Hietala, M. Melchionna, J. Helaja. *Adv. Synth. Catal.*, **357**, 3718 (2015).

[20] U. Berens, J.M. Brown, J. Long, R. Selke. *Tetrahedron: Asymm.*, **7**, 285 (1996).

[21] T.R. Li, M.M. Zhang, B.C. Wang, L.Q. Lu, W.J. Xiao. *Org. Lett.*, **20**, 3237 (2018).

[22] S. Naskar, P. Paira, R. Paira, S. Mondal, A. Maity, A. Hazra, K.B. Sahu, P. Saha, S. Banerjee, P. Luger, M. Webe, N.B. Mondal. *Tetrahedron*, **66**, 5196 (2010).

[23] J. Guo, J. Weng, G.B. Huang, L.J. Huang, A.S.C. Chan, G. Lu. *Tetrahedron Lett.*, **57**, 5493 (2016).

[24] H.A. Duong, S. Chua, P.B. Huleatt, C.L.L. Chai. *J. Org. Chem.*, **73**, 9177 (2008).

[25] B.O.A. Tasch, D. Antovic, E. Merkul, T.J.J. Müller. *Eur. J. Org. Chem.*, **2013**, 4564 (2013).

[26] J.E. Perea-Buceta, T. Wirtanen, O.V. Laukkanen, M.K. Mäkelä, M. Nieger, M. Melchionna, N. Huittinen, J.A.L. Sanchez, J. Helaja. *Angew. Chem. Int. Ed. Engl.*, **52**, 11835 (2013).

[27] M. Yamashita, T. Noro, A. Iida. *Tetrahedron Lett.*, **54**, 6848 (2013).

[28] B. Lal, A. Kanwal, A.A. Altaf, A. Badshah, F. Asghar, S. Akhter, S. Ullah, S.I. Khan, M.N. Tahir. *J. Coord. Chem.*, **72**, 2376 (2019).

[29] C. Díaz, G. Ferraudi, A.G. Lappin, A. Oliver, M. Isaacs. *J. Coord. Chem.*, **71**, 2584 (2018).

[30] Y.-Q. Hu, L.-M. Han, N. Zhu, H.-L. Hong, R.-J. Xie. *J. Coord. Chem.*, **66**, 3481 (2013).

[31] L.G. Yan, L.M. Han, R.J. Xie. *J. Coord. Chem.*, **72**, 2705 (2019).

[32] J.C. Torres, R.A. Pilli, M.D. Vargas, F.A. Violante, S.J. Garden, A.C. Pinto. *Tetrahedron*, **58**, 4487 (2002).

[33] M.J. Frisch, G.W. Trucks, H.B. Schlegel, G.E. Scuseria, M.A. Robb, J.R. Cheeseman. *Gaussian 09, Revision E.01*, Gaussian, Inc., Wallingford, CT (2013).

[34] A.D. Becke. *J. Chem. Phys.*, **98**, 5648 (1993).

[35] M. Dolg, U. Wedig, H. Stoll, H. Preuss. *J. Chem. Phys.*, **86**, 866 (1987).

[36] A. Schäfer, H. Horn, R. Ahlrichs. *J. Chem. Phys.*, **97**, 2571 (1992).

[37] Bruker, *APEX2 and SAINT-Plus*, Bruker AXS Inc., Madison, Wisconsin (2004).

[38] G.M. Sheldrick. *Acta Crystallogr. C Struct. Chem.*, **71**, 3 (2015).

[39] A. Arcadi, G. Bianchi, F. Marinelli. *Synthesis*, **4**, 610 (2004).

[40] J.P. Hurvois, C. Moinet. *J. Organomet. Chem.*, **690**, 1829 (2005).

[41] L.Z. Zhang, H. Chen, X.F. Zhao, Q. Zhai, D.J. Yin, Y.F. Sun, J.H. Li. *Appl. Catal. B: Environ.*, **193**, 47 (2016).

[42] T.G. Costa, B. Szpoganicz, G.F. Caramori, V.R. de Almeida, A.S. Mangrich, A.P. Mangoni. *J. Coord. Chem.*, **67**, 986 (2014).

[43] Y. Okada, T. Nakagawa, T. Hayashi. *Inorg. Chim. Acta*, **312**, 197 (2001).

[44] Q. Wang, S.L. Tian, P. Ning. *Ind. Eng. Chem. Res.*, **53**, 643 (2014).

[45] Y.J. Li, B.J. Zhang, X.L. Liu, Q. Zhao, H. Zhang, Y.C. Zhang, P. Ning, S.L. Tian. *J. Hazard. Mater.*, **353**, 26 (2018).

[46] C.K. Duesterberg, S.E. Mylon, T.D. Waite. *Environ. Sci. Technol.*, **42**, 8522 (2008).

[47] Q. Wang, S.L. Tian, J. Cun, P. Ning. *Desal. Water Treat.*, **51**, 5821 (2013).

[48] G. Abbiati, F. Marinelli, E. Rossi, A. Arcadi. *Isr. J. Chem.*, **53**, 856(2013).